

Voltage interval mappings for an elliptic bursting model

Jeremy Wojcik and Andrey Shilnikov

Abstract We employed Poincaré return mappings for a parameter interval to an exemplary elliptic bursting model, the FitzHugh-Nagumo-Rinzel model. Using the interval mappings, we were able to examine in detail the bifurcations that underlie the complex activity transitions between: tonic spiking and bursting, bursting and mixed-mode oscillations, and finally, mixed-mode oscillations and quiescence in the FitzHugh-Nagumo-Rinzel model. We illustrate the wealth of information, qualitative and quantitative, that was derived from the Poincaré mappings, for the neuronal models and for similar (electro)chemical systems.

1 Introduction

The class of elliptic bursting models is rich and can be found in diverse scientific studies, ranging from biological systems [1] to chemical processes such as the Belousov-Zhabotinsky reaction [2]. Transitions between activity states for elliptic bursting models is not common knowledge. Often in the sciences specialization leads to discoveries that remain unknown in other branches of science; the recent reincarnation of mixed mode oscillations (MMO) in neuroscience for example. In neuroscience, transitions in activity revolve around a changing membrane potential and specific changes in potential may instigate the onset of a seizure in the case of epilepsy or determine muscle reactions in response to stimulus. The class of elliptic bursting models needs a more general treatment that can span multiple disciplines.

Jeremy Wojcik

Neuroscience Institute, and Department of Mathematics and Statistics, Georgia State University, Atlanta, 100 Piedmont Ave SE, Atlanta, GA, 30303, USA e-mail: jwojcik1@gsu.edu

Andrey Shilnikov

Neuroscience Institute, and Department of Mathematics and Statistics, Georgia State University, Atlanta, 100 Piedmont Ave SE, Atlanta, GA, 30303, USA e-mail: ashilnikov@gsu.edu

We propose a case study of the phenomenological FitzHugh-Nagumo-Rinzel model in order to investigate the mechanisms for state transitions in dynamic behavior.

Bursting represents direct evidence of multiple time scale dynamics of a model. Deterministic modeling of bursting models was originally proposed and done within a framework of three-dimensional, slow-fast dynamical systems. Geometric configurations of models of bursting neurons were pioneered by Rinzel [3, 4] and enhanced in [5, 6]. The proposed configurations are all based on the geometrically comprehensive dissection approach or the time scale separation which has become the primary tools in mathematical neuroscience. The topology of the slow motion manifolds is essential to the geometric understanding of dynamics. Through the use of geometric methods of the slow-fast dissection, where the slowest variable of the model is treated as a control parameter, it is possible to detect and follow the manifolds made of branches of equilibria and limit cycles in the fast subsystem. Dynamics of a slow-fast system are determined by, and centered around, the attracting sections of the slow motion manifolds [7, 8, 9, 10].

The slow-fast dissection approach works exceptionally well for a multiple time scale model, provided the model is far from a bifurcation in the singular limit. On the other hand, a bifurcation describing a transition between activities may occur from reciprocal interactions involving the slow and fast dynamics of the model. Such slow-fast interactions may lead to the emergence of distinct dynamical phenomena and bifurcations that can occur only in the full model, but not in either subsystem of the model. As such, the slow-fast dissection fails at the transition where the solution is no longer constrained to stay near the slow motion manifold, or when the time scale of the dynamics of the fast subsystem slows to that of the slow system, near the homoclinic and saddle node bifurcations for example.

Transformative bifurcations of repetitive oscillations, such as bursting, are most adequately described by Poincaré mappings [11], which allow for global bifurcation analysis. Time series based Poincaré mappings have been heavily employed for examinations of voltage oscillatory activities in a multitude of applied sciences [12, 13, 14], despite their limitation due to sparseness. Often, feasible reductions to mappings of the slowest variable can be achieved through the aforementioned dissection tool in the singular limit [15, 16, 17, 11]. However, this method often fails for elliptic bursters since no single valued mapping for the slow variable can be derived for the particular slow motion manifold.

In this paper, we refine and expound on the technique of creating a family of one-dimensional mappings, proposed in [18, 19, 20], for the leech heart interneuron, into the class of elliptic models of endogenously bursting neurons. We will show that a plethora of information, both qualitative and quantitative can be derived from the mappings to thoroughly describe the bifurcations as such a model undergoes transformations. We also demonstrate the power of deriving not only individual mappings, but the additional benefits of having the entire family of mappings created from an elliptic bursting model.

2 FitzHugh-Nagumo-Rinzel Model

We introduce the exemplary phenomenological elliptic bursting model, the FitzHugh-Nagumo-Rinzel model. The model exhibits all necessary traits for the class of elliptic bursters: the time series form elliptic shaped bursts and oscillations are begin through an Andronov-Hopf bifurcation and end in a saddle-node bifurcation. The model exhibits several types of oscillations including: constant high amplitude oscillatory behavior (tonic spiking), bursting, low amplitude oscillations, and MMO. The mathematical FitzHugh-Nagumo-Rinzel model of the elliptic burster is given by the following system of equations with a single cubic nonlinear term:

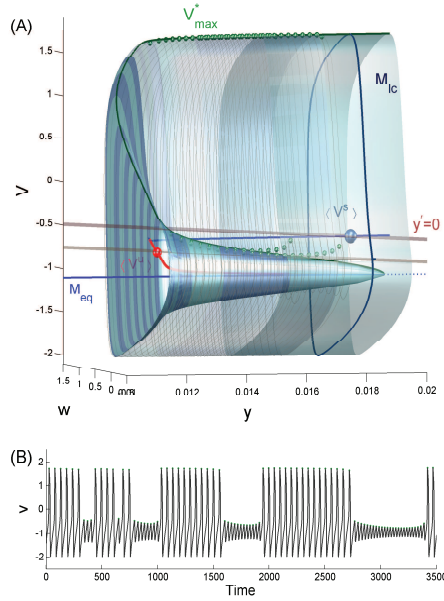


Fig. 1: (A) Topology of the tonic spiking, M_{lc} , and quiescent, M_{eq} manifolds. Solid and dashed branches of M_{eq} are made of stable and unstable equilibria of the model, resp. The space curve, labeled by V_{max}^* (in green), corresponds to the v -maximal coordinates of the periodic orbits composing M_{lc} . An intersection point of $y' = 0$ with M_{eq} is an equilibrium state of (1). Shown in grey is the bursting trajectory traced by the phase point: the number of spikes per burst is the same as the number of turns the phase point makes around M_{lc} . Spikes are interrupted by the periods of quiescence when the phase point follows M_{eq} after it falls from M_{lc} near the fold. (B) A voltage trace for $c = -0.67$ displaying the voltage evolution in time as the phase point travels around the slow motion manifolds.

$$\begin{aligned}
v' &= v - v^3/3 - w + y + I, \\
w' &= \delta(0.7 + v - 0.8w), \\
y' &= \mu(c - y - v);
\end{aligned} \tag{1}$$

here we fix $\delta = 0.08$, $I = 0.3125$ is an applied external current, and $\mu = 0.002$ is a small parameter determining the pace of the slow y -variable. The slow variable, y , becomes frozen in the singular limit, $\mu = 0$. We employ c as the primary bifurcation parameter of the model, variations of which elevate/lower the slow nullcline given by $y' = 0$. The last equation is held geometrically in a plane given by $v = y - c$ in the three-dimensional phase space of the model, see Fig. 1. The two fast equations in (1) describe a relaxation oscillator in a plane, provided δ is small. The fast subsystem exhibits either tonic spiking oscillations or quiescence for different values of y corresponding to a stable limit cycle and a stable equilibrium state, respectively. The periodic oscillations in the fast subsystem are caused by a hysteresis induced by the cubic nonlinearity in the first “voltage” equation of the model.

Fig. 1 (A) presents a 3D view of the slow motion manifolds in the phase space of the FitzHugh-Nagumo-Rinzel model. The tonic spiking manifold M_{lc} is composed of the limit cycles for the model (1), both stable (outer) and unstable (inner) sections. The fold on M_{lc} corresponds to a saddle-node bifurcation, where the stable and unstable branches merge. The vertex, where the unstable branch of M_{lc} collapses at M_{eq} , corresponds to a subcritical Andronov-Hopf bifurcation. The manifold M_{eq} is the space curve made from equilibria of the model. The intersection of the plane, $y' = 0$ with the manifold, determines the location of the existing equilibrium state for a given value of the bifurcation parameter c : stable (saddle-focus) if located before (after) the Andronov-Hopf bifurcation point on the solid (dashed) segment of M_{eq} . The plane, $y' = 0$, called the slow nullcline, above (below) which the y -component of a solution of the model increases (decreases). The plane moves in the 3D phase space as the control parameter c is varied. When the slow nullcline cuts through the solid segment of M_{eq} , the model enters a quiescent phase corresponding to a stable equilibrium state. Raising the plane to intersect the unstable (inner) cone-shaped portion of M_{lc} makes the equilibrium state unstable through the Andronov-Hopf bifurcation, which is subcritical in the singular limit, but becomes supercritical at a given value of the small parameter $\varepsilon = 0.002$, see Fig. 1(A). Continuing to raise the slow nullcline by increasing c gives rise to bursting represented by solutions following and repeatedly switching between M_{eq} and M_{lc} . Bursting occurs in the model (1) whenever the quiescent M_{eq} and spiking M_{lc} manifolds contain no attractors, i.e. neither a stable equilibrium state nor a stable periodic orbit exist. The number of complete revolutions, or “windings”, of the phase point around M_{lc} corresponds to the number of spikes per burst. The larger the number of revolutions the longer the active phase of the neuron lasts. Spike trains are interrupted by periods of quiescence while the phase point follows the branch M_{eq} , onto which the phase point falls from M_{lc} near the fold, see Fig. 1. The length of the quiescent period, as well as the delay of the stability loss (determined mainly, but not entirely, by the small parameter μ) begins after the phase point passes through the subcritical Andronov-Hopf bifurcation onto the unstable section of M_{eq} . Further increase of the bifurcation parameter,

c , moves the slow nullcline up so that it cuts through the stable cylinder-shaped section of the manifold M_{lc} far from the fold. This gives rise to a stable periodic orbit corresponding to tonic spiking oscillations in the model.

3 Voltage interval mappings

Methods of the global bifurcation theory are organically suited for examinations of recurrent dynamics such as tonic spiking, bursting and subthreshold oscillations [21, 22], as well as their transformations. The core of the method is a reduction to, and derivation of, a low dimensional Poincaré return mapping with an accompanying analysis of the limit solutions: fixed, periodic and homoclinic orbits each representing various oscillations in the original model. and referenced therein. It is customary that such a mapping is sampled from time series, such as identification of voltage maxima, minima, or interspike intervals [23], Fig. 1(B). A drawback of a mapping generated by time series is sparseness as the construction algorithm reveals only a single periodic attractor of a model, unless the latter demonstrates chaotic or mixing dynamics producing a large set of densely wandering points. Chaos may also be evoked by small noise whenever the dynamics of the model are sensitively vulnerable to small perturbations that do not substantially re-shape intrinsic properties of the autonomous model [20, 24]. Small noise, however, can make the solutions of the model wander thus revealing the mapping graph.

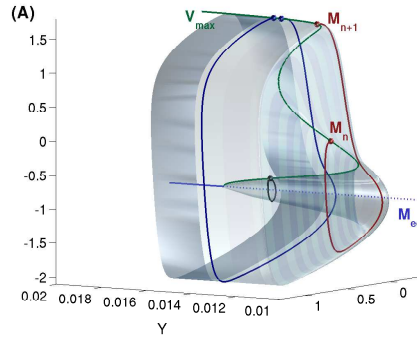


Fig. 2: Three sample orbits demonstrating the construction of the return mapping $T: M_n \rightarrow M_{n+1}$ defined for the points of the cross-section V_{\max} on the manifold M_{lc} . Singling out the v -coordinates of the points gives pairs (V_n, V_{n+1}) constituting the voltage interval mapping at a given parameter, c .

A computer assisted method for constructing a complete family of Poincaré mappings for an interval of membrane potentials was proposed in [19] following [25]. Having a family of such mappings we are able to elaborate on various bifurcations of periodic orbits, examine bistability of coexisting tonic spiking and bursting, and detect the separating unstable sets that are the organizing centers of complex dynamics in any model. Examination of the mappings will help us make qualitative predictions about transitions *before* the transitions occur in models.

By construction, the mapping T takes the space curve V_{\max}^* into itself after a single revolution around the manifold M_{lc} , Fig. 2, i.e. $T : V_n \rightarrow V_{n+1}$. This technique allows for the creation of a Poincaré return mapping; taking an interval of the voltage values into itself. The found set of matching pairs (V_n, V_{n+1}) constitutes the graph of the Poincaré mapping for a selected parameter value c . Provided the number of paired coordinates is sufficiently large and by applying a standard spline interpolation we are able to iterate trajectories of the mapping, compute Lyapunov exponents, evaluate the Schwarzian derivative, extract kneading invariants for the topological entropy, and determine many other quantities.

Varying the parameter, c , we are able to obtain a dense family that covers all behaviors, bifurcations and transitions of the model (1). A family of the mappings for the parameter, c , varied within the range $[-1, -0.55]$ is shown in Fig. 3. Indeed, for the sake of visibility, this figure depicts a sampling of mappings that indicate evolutionary tendencies of the model. A thorough examination of the family allows us to foresee changes in model dynamics. A family of mappings allows us to analyze all the bifurcations whether stable or unstable fixed and periodic orbits including homoclinic and heteroclinic orbits and bifurcations. By following the mapping graph we can predict a value of the parameter at which the corresponding periodic orbit will lose stability or vanish, for example giving rise to bursting from tonic spiking.

A fixed point, v^* , is discerned from the mapping as an intersection of the graph with the bisectrix. Visually we determine the stability of the fixed point by the slope of the graph at the fixed point. If the slope of the graph is less than 1 in absolute value the point is stable. When the absolute value of the slope of the graph at the fixed point is greater than 1 the fixed point is unstable. Alternatively stability may be determined from forward iterates of an initial point in the neighborhood of the fixed point which converges to the fixed point.

4 Qualitative analysis of mappings

The family of mappings given in Fig. 3 allows for global evolutionary tendencies of the model (1) to be qualitatively analyzed. One can first see that the flat mappings in grey have a single fixed point corresponding to the tonic spiking state. The green mappings show the actual transition and saddle-node bifurcation after which we have regular bursting patterns, seen in the blue mappings. We also see the other unstable fixed point clearly moving to the lower corner. The red mappings indicate the transition from bursting to quiescence, as the fixed point changes stability.

A major benefit of using the voltage interval mapping is that we are able to understand transitions between the activity states of the model by analyzing and comparing the bifurcations between the states. Activity transitions commonly occur in a slow-fast model near the bifurcations of the fast subsystem where the description of dynamics in the singular limit is no longer accurate because of the failure of (or interpretation of) the slow-fast dissection paradigm. This happens, for example, when the two-dimensional fast subsystem of the model (1) is close to a saddle-node bifurcation (near the fold on the tonic spiking manifold M_{lc}) where the fast dynamics slow to the time scale of the slow subsystem. Such an interaction may cause new and peculiar phenomena such as torus formation and subsequent breakdown near the fold on the spiking manifold [26, 27]. We now turn our attention to a more thorough analysis of the individual mappings.

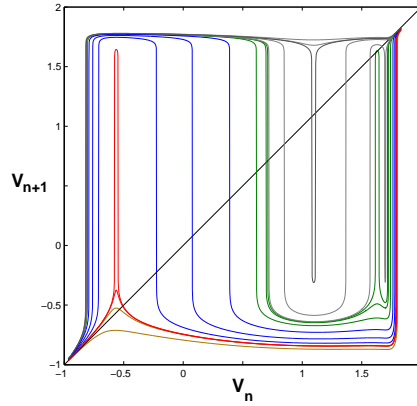


Fig. 3: Coarse sampling of the c -parameter family of the Poincaré return mappings $T : V_n \rightarrow V_{n+1}$ for the FitzHugh-Nagumo-Rinzel model at $\mu = 0.002$ as c decreases from $c = -0.55$ through $c = -1$. The grey mappings correspond to the dominating tonic spiking activity in the model. The green mappings show the model transitioning from tonic spiking to bursting. The blue mappings correspond to the bursting behavior in the model. The red mappings show the transition from bursting into quiescence. The orange mappings correspond to the quiescence in the model. An intersection point of a mapping graph with the bisectrix is a fixed point, v^* , of the mapping. The stability of the fixed point is determined by the slope of the mapping graph, i.e. it is stable if $|T'(v^*)| < 1$. Nearly vertical slopes of graph sections are due to an exponentially fast rate of instability of solutions (limit cycles) of the fast subsystem compared to the slow component of the dynamics of the model.

4.1 Transition from tonic spiking to bursting

We begin where the model is firmly in the tonic spiking regime at $c = -0.594355$. Tonic spiking is caused by the presence of a stable periodic orbit located far from the fold on the manifold M_{lc} (Fig. 1). The only v -maximum of this orbit corresponds to a stable fixed point, labeled TS in Fig. 4(A). The flat section of the mapping graph adjoining the stable fixed point clearly indicates a rapid convergence to the point in the v -direction, as shown by the trace in inset (B). Here the slope of the mapping reflects the exponential instability (stability) of the quiescent (tonic spiking) branch, made of unstable equilibria and stable limit cycles of the fast subsystem of the model.

The formation of the cusp is an indication of a change in dynamics for the mapping. Thus the mapping insinuates a transition in dynamics of the model (1) prior to occurance. Note that the maximal voltage trace provides no indication of any emi-

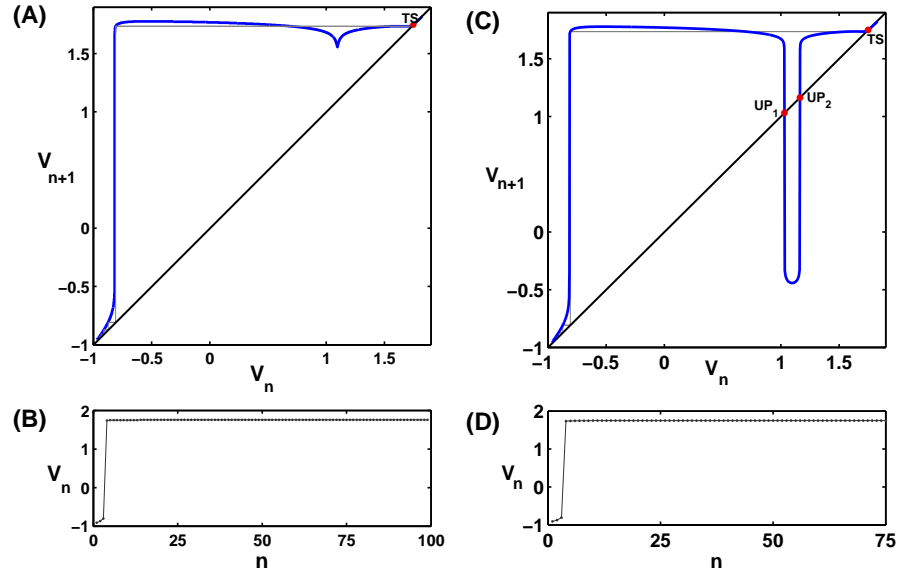


Fig. 4: (A) Poincaré return mapping for the parameter, $c = -0.594255$. We see a single fixed point, TS, corresponding to continuous large amplitude oscillations. We also see a cusp which insinuates a possible change in the mapping shape. (B) A maximal “time” series obtained from iterating the mapping, n times. (C) Return mapping for $c = -0.595$. We see the cusp has enlarged and intersected the identity line creating 2 additional fixed points, UP_1 and UP_2 . The two fixed points are clearly unstable. (D) There is no indication in the maximal trace, or model dynamics, that would indicate the formation of these fixed points.

ment transition in the model's behavior. The mapping in Fig. 4(A, B), taken for the parameter $c = -0.595$, clearly illustrates that after the cusp has dropped below the bisectrix, two additional fixed points, UP_1 and UP_2 , are created. UP_1 and UP_2 have emerged through a preceding fold or saddle-node bifurcation taking place at some intermediate parameter value between $c = -0.594255$ and $c = -0.595$. Again, let us stress that the singular limit of the model at $\mu = 0$ gives a single saddle-node bifurcation through which the tonic spiking periodic orbit loses stability after it reaches the fold on the tonic spiking manifold. We point out that, for an instant, the model becomes bistable right after the saddle-node bifurcation in Fig. 4 leading to the emergence of another stable fixed point with an extremely narrow basin of attraction. Here, as before the hyperbolic tonic spiking fixed point, TS, dominates the dynamics of the model.

Figure 5(A) demonstrates that, as the parameter is decreased further to $c = -0.615$, the gap between the new fixed points widens as the point UP_2 moves toward the stable tonic spiking point, TS, indicating a possible saddle-node bifurcation is eminent. Through this saddle-node bifurcation, these fixed points merge and annihilate each other; thereby terminate the tonic spiking activity in the FitzHugh-Nagumo-Rinzel model. Before that happens however, several bifurcations involving

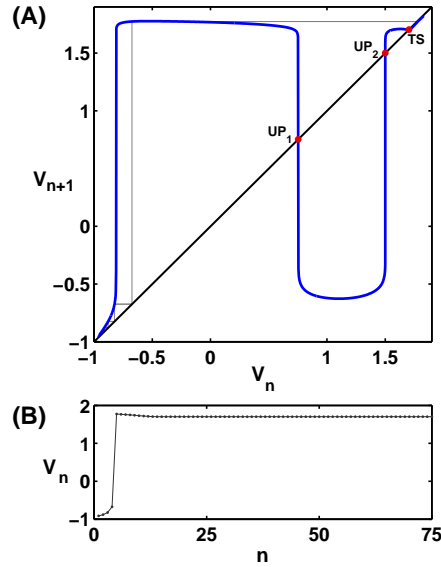


Fig. 5: (A) Varying the parameter further to $c = -0.615$ we find the unstable fixed point UP_2 has moved closer to the stable fixed point, TS. The other unstable fixed point UP_1 remains in approximately the same location. (B) Again the maximal trace shows no indication of any change in dynamics.

the fixed point, TS, drastically reshape the dynamics of the model. First, the multiplier becomes negative around $c = -0.619$, which is the first indication of an impending period doubling cascade. This is confirmed by the mapping at $c = -0.6193$ in Fig. 6(A, B C) showing that the fixed point has become unstable through the supercritical period-doubling bifurcation. Furthermore, the dynamics of the mapping is directly mimicked in the full model behavior, see Fig 6(D)

The new born period-2 orbit becomes the new tonic spiking attractor of the mapping. Observe from the voltage trace in Fig. 6(B) the long transient bursting behavior thus indicating that boundaries of the attraction basin of the period-two orbit become fractal. Next, the model approaches bursting onset. Correspondingly, the FitzHugh-Nagumo Rinzel model starts generating chaotic trains of bursts with randomly alternating numbers of spikes per burst. The number of spikes depends on how close the trajectory of the mapping comes to the unstable (spiraling out) fixed point, TS, that is used to represent the tonic spiking activity. Each spike train is in-

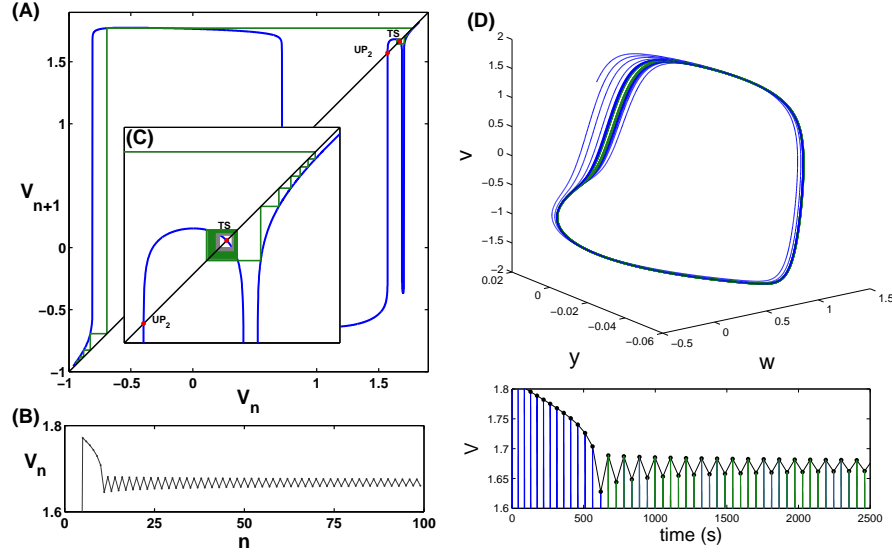


Fig. 6: (A) Poincaré mapping at $c = -0.6193$ and the voltage trace in (B) both demonstrate chaotic bursting transients. (C) Enlargement of the right top corner of the mapping shows that the tonic spiking fixed point has lost the stability through a supercritical period-doubling bifurcation. The new born period-2 orbit is a new attractor of the mapping, as confirmed by the zigzagging voltage trace represented in (B). (D) The same dynamics found directly from integrating the model. We find after a short transient (blue) the model dynamics converge to a period 2 orbit (green) as indicated from the mapping (A).

interrupted by a single quiescent period. The unstable point, UP_1 , corresponds to a saddle periodic orbit of the model that is located on the unstable, cone-shaped section of the tonic spiking manifold M_{IC} in Fig. 1. Recall that this saddle periodic orbit is repelling in the fast variables and stable in the slow variable.

By comparing Figs. 4-7 one could not foresee that the secondary saddle-node bifurcation eliminating the tonic spiking fixed point TS, or corresponding round stable periodic orbit on the manifold M_{IC} would be preceded by a dramatic concavity change in the mapping shape causing a forward and inverse cascade of period doubling bifurcations right before the tonic spiking orbit TS. The corresponding fixed point, TS, becomes stable again through a reverse sequence of period doubling bifurcations before annihilating through the secondary saddle-node bifurcation. However, the basin of attraction becomes so thin that bursting begins to dominate the bi-stable dynamics of the model. Note that the bursting behavior becomes regular as the phase points pass through the upper section of the mapping tangent to the bisectrix. The number of iterates that the orbit makes here determine the duration of the tonic spiking phase of bursting and is followed by a quiescence period initially comprised of a single iterate of the phase point to the right of the threshold

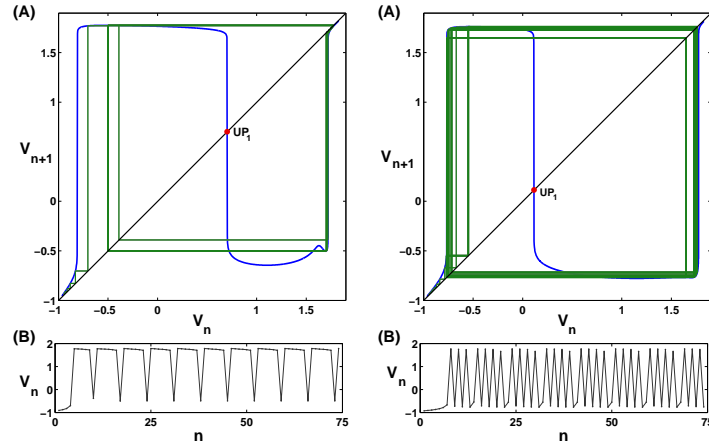


Fig. 7: (A) Periodic bursting with five spikes in the Poincaré interval mapping for the FitzHugh-Nagumo-Rinzel model at $c = -0.6215$. The single unstable fixed point UP_1 separates the tonic spiking section of the mapping from the quiescent or subthreshold section (left). The number of iterates of the phase point adequately defines the ordinal type of bursting (B). Note a presence of a small hump around $(V_0 = 1.6, V_1 = -0.5)$ which is an echo of the saddle-node bifurcation. (C) Poincaré return mapping at $c = -0.75$. Here we find a burst pattern of 3 spikes followed by 2 small amplitude oscillations. The mappings are able to capture all the bursting patterns exhibited by the model.

UP_1 . The evolution of bursting into MMO and on to subthreshold oscillations will be discussed in the next section.

4.2 From bursting to mixed-mode oscillations and quiescence

The disappearance of the tonic spiking orbit, TS, accords with the onset of regular bursting in the mapping and in the model (1). In the mapping, a bursting orbit is comprised of iterates on the tonic spiking and quiescent sections separated by the unstable threshold fixed point, UP_1 , of the mapping in Fig. 7. The shape of the graph undergoes a significant change reflecting the change in dynamics. The fixed points in the upper right section of the mapping disappear through a saddle-node bifurcation. One of the features of the saddle-node is the bifurcation memory: the phase point continues to linger near a phantom of the disappeared saddle-node. The

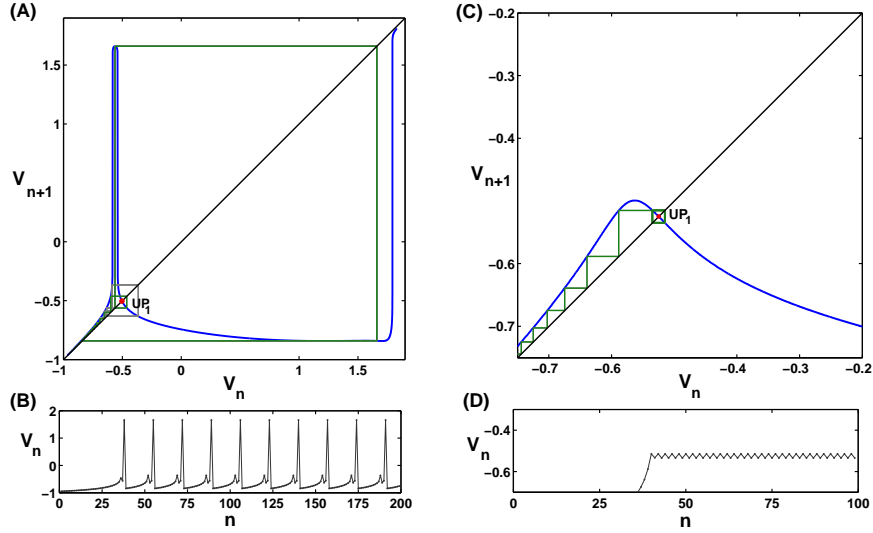


Fig. 8: (A) Chaotic MMO and bursting in the mapping at $c = -0.904$ caused by the complex recurrent behavior around the unstable fixed point UP_1 . (B) Subthreshold oscillations are disrupted sporadically by large and intermediate magnitude spikes thereby destroying the rhythmic bursting in the model. (C) Poincaré return mapping for the FitzHugh-Nagumo-Rinzel model shows no bursting but complex subthreshold period 2 oscillations at $c = -0.908$. (D) After the peak in the mapping decreases in amplitude, high amplitude spikes becomes impossible. Here, chaos is caused by homoclinic orbits to the unstable fixed point UP_1 , just prior to this figure.

mapping near the bisectrix can generate a large number of iterates before the phase points diverge toward the quiescent phase. The larger the number of iterates near the bisectrix corresponds to a longer tonic spiking phase of bursting. Figure 7 demonstrates how the durations of the phases change along with a change in the mapping shape: from a single quiescent iterate to the left of the threshold, UP_1 , to a single tonic-spiking iterate corresponding to a bursting orbit with a single large spike in the model.

The transition from bursting to quiescence in the model is not monotone because the regular dynamics may be sparked by episodes of chaos. Such subthreshold chaos in the corresponding mapping at $c = -0.9041$ is demonstrated in Fig. 8(A). This phenomena is labeled MMO because the small amplitude subthreshold oscillations are sporadically interrupted by larger spikes (Inset B). Use of the mapping makes the explanation of the phenomena in elliptic bursters particularly clear. In Fig. 8(A), after the mapping (or the model) fires a spike, the phase point is reinjected close to the threshold point, UP_1 , from where it spirals away to make another cycle of bursting. Note that the number of iterates of the phase point around UP_1 may vary after each spiking episode. This gives rise to solutions that are called bi-asymptotic or homoclinic orbits to the unstable fixed point UP_1 . The occupancy of such a homoclinic orbit to a repelling fixed point is the generic property of a one-dimensional non-invertible mapping [28], since the point of a homoclinic orbit might have two pre-images. Note that the number of forward iterates of a homoclinic point may be finite in a non-invertible mapping, because the phase point might not converge, but merely jump onto the unstable fixed point after being reinjected. However, the number of backward iterates of the homoclinic point is infinite, because the repelling fixed point becomes an attractor for an inverse mapping in restriction to the local section of the unimodal mapping, see Fig. 8(A, B). The presence of a single homoclinic orbit leads to the abundance of other emergent homoclinics [29] via a homoclinic explosion [11].

A small decrease of the bifurcation parameter causes a rapid change in the shape of the mapping, as depicted in Figs. 8(C, D). The sharp peak near the threshold becomes lower so that the mapping can no longer generate large amplitude spikes. As the parameter is decreased further, the unstable fixed point, UP_1 , becomes stable through a reverse period-doubling cascade. The last two stages of the cascade are depicted in Fig. 9. Insets (A) and (C) of the figure show stable period-4 and period-2 orbits, and their traces in Insets (B) and (D), as the parameter c is decreased from -0.906 to -0.9075 . Here we demonstrate another ability of the interval mappings derived directly from the flow. In addition to the original mapping, T , in Fig. 9 we see two superimposed mappings, T^2 and T^4 , (shown in light blue) of degree two and four respectively. The four points of periodic orbit in Inset (A) corresponds to the four fixed points of the fourth degree mapping T^4 at $c = -0.9075$, whereas the period-two orbit in (C) correspond to two new fixed points of the mapping T^2 in (C) at $c = -0.9075$. We see clearly that both periodic orbits are indeed stable because of the slopes of the mappings at the fixed points on the bisectrix. Using the mappings of higher degrees we can evaluate the critical moments at which the period-two and period-four orbits are about to bifurcate. We point out that a period-

doubling cascade, beginning with a limit cycle near the Hopf-initiated canard toward subthreshold chaos has been recently reported in slow-fast systems [30, 31].

Decreasing c further, the period-two orbit collapses into the fixed point, UP_1 , which becomes stable. The multiplier, first negative becomes positive but is still less than one in the absolute value. In terms of the model, this means that the periodic orbit collapses into a saddle-focus through the subcritical Andronov-Hopf bifurcation. After that, the equilibrium state, located at the intersection of the manifold M_{eq} with the slow-nullcline (plane) in Fig. 1, becomes stable and the model goes into quiescence for parameter values smaller then $c = -0.97$. The stable equilibrium state corresponds to the fixed point, Q , which is the global attractor in the mapping.

5 Quantitative features of mappings: Kneadings

In this section we discuss a quantitative property of the interval mappings for the dynamics of the model (1). In particular, we carry out the examination of complex dynamics with the use of calculus-based and calculus-free tools such as Lyapunov exponents and kneading invariants for the symbolic description of MMOs.

Chaos may be quantitatively measured by a Lyapunov exponent. The Lyapunov exponent is evaluated for the one-dimensional mappings as follows:

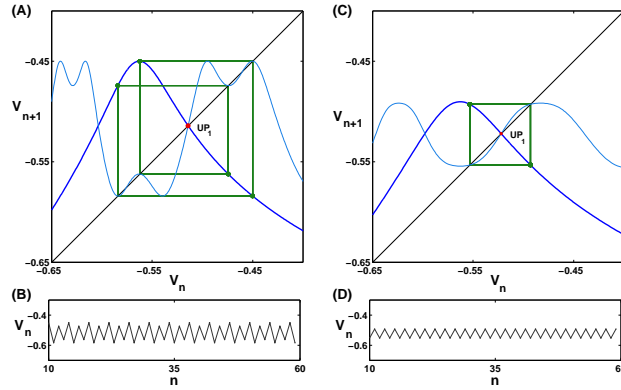


Fig. 9: (A) and (C) Show stable period-4 and period-2 orbits (green) of the interval mapping at $c = -0.906$ and $c = -0.9075$. Shown in light-blue are the corresponding mappings T^4 and T^2 of degree four and two with four and two stable fixed points correspondingly. The traces of the orbits are shown in Insets (B) and (D).

$$\lambda = \lim_{N \rightarrow +\infty} \frac{1}{N} \sum_{i=1}^N \log |T'(v_i)|, \quad (2)$$

where $T'(v_i)$ is the slope (derivative) of the mapping at the current iterate v_i corresponding to the i -th step for $i = 0, \dots, N$. Note that, by construction, the mapping graph is a polygonal and to accurately evaluate the derivatives in (5) we used a cubic spline. The Lyapunov exponent, λ , yields a lower bound for the topological entropy $h(T)$ [32]; serving as a measure of chaos in a model. The Lyapunov exponent values $\lambda \simeq 0.24$ and $\lambda \simeq 0.58$, found for the interval mappings at $c = -0.9041$ and $c = -0.90476$, resp., show that chaos is developed more in the case of subthreshold oscillations than for MMOs.

The topological entropy may also be evaluated through a symbolic description of the dynamics of the mapping that require no calculus-based tools. The curious reader is referred to [33, 34] for the in-depth and practical overviews of the kneading invariants, while below we will merely touch the relevant aspects of the theory. For unimodal mappings of an interval into itself with a single critical point, v_c , like for the case $c = -0.90476$, we need only to follow the forward iterates of the critical point to generate the *unsigned kneading sequence* $\kappa(v_c) = \{\kappa_n(v_c)\}$ defined on $\{-1, +1\}$ by the following rule:

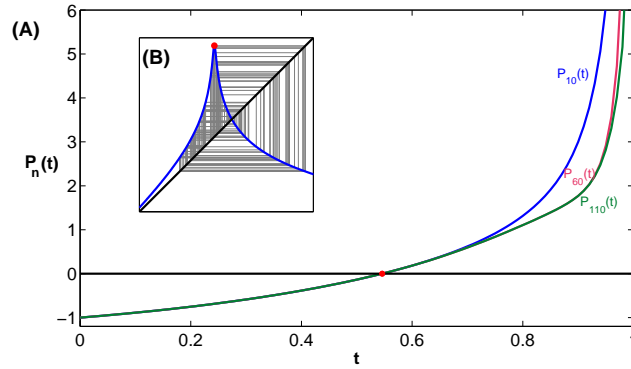


Fig. 10: (A) Graphs of the three polynomials, $P_{10}(t)$, $P_{60}(t)$ and $P_{110}(t)$ defined on the unit interval, and generated through the series of the signed kneadings at $c = -0.90476$. Inset (B) shows the corresponding interval mapping. The iterates of the critical point, v_c , determine the symbolic dynamics for the unsigned kneading symbols: -1 if the the phase point lands on the decreasing section of the mapping graph to the right of the critical point, and $+1$ if it lands to the increasing section of the mapping, which is to the left of the critical point.

$$\kappa_n(v_q) = \begin{cases} +1, & \text{if } T^n(v_c) < v_c \\ -1, & \text{if } T^n(v_c) > v_c; \end{cases} \quad (3)$$

here $T^n(v_c)$ is the n -th iterate of the critical point v_c .

The kneading invariant of the unimodal mapping is a series of the *signed kneadings* $\{\tilde{\kappa}_n\}$ of the critical point, which are defined through the unsigned kneadings, κ_i , as follows:

$$\tilde{\kappa}_n = \prod_{i=1}^n \kappa_i, \quad (4)$$

or, recursively:

$$\tilde{\kappa}_n = \kappa_n \tilde{\kappa}_{n-1}, \quad i = 2, 3, \dots \quad (5)$$

Next we construct a formal power series;

$$P(t) = \sum_{i=0}^{\infty} \tilde{\kappa}_i t^i. \quad (6)$$

The smallest zero, t^* (if any), of the series within an interval $t \in (0, 1)$ defines the topological entropy, $h(T) = \ln(1/t^*)$. The sequence of the signed kneadings, truncated to the first ten terms, $\{- + + + - + + + - +\}$ for the mapping in Fig. 10 inset B, generates the polynomial $P_{10}(t) = -1 + t + t^2 + t^3 - t^4 + t^5 + t^6 + t^7 - t^8 + t^9$. The single zero of $P_{10}(t)$ at $t^* \approx 0.544779$ yields a close estimate for the topological entropy $h(T) \approx 0.6073745$, see Fig. 10(A). The advantage of an approach based on the kneading invariant to quantify chaos is that evaluation of the topological entropy does not involve numerical calculus for such equationless interval mappings, but relies on the mixing properties of the dynamics instead. Moreover, it requires relatively few forward iterates of the critical point to compute the entropy accurately, as the polynomial graphs in Fig. 10 suggests. Besides yielding the quantitative information such as the topological entropy, the symbolic description based on the kneading invariants provide qualitative information for identifying the corresponding Farey sequences describing the MMOs in terms of the numbers of subthreshold and tonic spiking oscillations.

6 Discussion

We present a case study for an in-depth examination of the bifurcations that take place at activity transitions between tonic spiking, bursting and Mixed Mode Oscillations in the FitzHugh-Nagumo-Rinzel model. The analysis is accomplished through the reduction to a single-parameter family of equationless Poincaré return mappings for an interval of the “voltage” variable. We stress that these mappings are *models* themselves for evaluating the complex dynamics of the full three-dimensional model. Nevertheless, the dynamics of the single accumulative variable, v , reflects the cooperative dynamics of other variables in the model. The reduc-

tion is feasible since the model is a slow-fast system and, hence, possesses a two-dimensional, slow-motion tonic-spiking manifold around which the oscillatory solutions of the models linger. We have specifically concentrated on the dynamics of the voltage [18, 20], as it is typically the only measurable, and thus comparable, variable in experimental studies in neuroscience and physical chemistry.

It is evident that no 1D return mapping of the interval is intended to detect a torus in the phase plane, whereas the pointwise mappings generated by a forward time series of the voltage can identify the torus formation in the phase space. Note that the torus has a canard-like nature, that is the torus exists within a narrow parameter window. A torus formation in a 3D model with two slow variables near the fold was reported also in [35]. Another parallel of the FitzHugh-Nagumo-Rinzel model with electrochemical systems, including the Belousov-Zhabotinsky reaction, is that the latter also demonstrates a quasiperiodic regime [2]. The emergence of the torus near the fold of the tonic spiking manifold first described in [27, 36] has turned out to be a generic phenomenon observed recently in several plausible models [37, 38], including a model for the Purkinje cells [26, 39], and in a 12D hair cell model [40]

A minor drawback of the approach is a small detuning offset in parameter values at which the model and the mapping have nearly the same dynamics, matching orbits, or undergo the same bifurcations. This is caused by the fact that a one-dimensional mapping for a single voltage variable does not fully encompass the dynamics of other, major and minor, variables of the corresponding model. In general, most features of a dissipative model with a negative divergence of the vector field that results in a strong contraction of the phase volumes, are adequately modeled by a 1D Poincaré mapping. However, this is not true when such a contraction is no longer in place, for example, when the divergence becomes sign-alternating. There are two such places near the manifold M_{lc} in the model (1): one is near the fold, the second is close to the cone-shaped tip. The sign alternating near the tip of the cone is where the model has an equilibrium state of the saddle-focus type with a pair of complex conjugate eigenvalues with a small positive real part and a real negative eigenvalue due to the Andronov-Hopf bifurcation and the smallness of ε .

The algorithm for interval mapping construction has two stages. First, one needs to identify the tonic spiking manifold in the phase space of the slow-fast neuron model in question. This is accomplished by either using the geometric dissection method, or the parameter continuation technique. The more accurately and completely the first stage is performed the more natural and smooth these numerically derived mappings will be. The second stage is to build the mappings for a range of parameter values. The analysis of such mappings lets one identify not only attractors, but more importantly, the unstable sets including fixed, periodic and homoclinic orbits, which are known to be the globally organizing centers governing the dynamics of any model. In addition, having computationally smooth mappings allows one to create symbolic descriptions for dynamics, compute kneading invariants, evaluate Schwarzian derivatives etc., as well as estimate other quantities measuring the degree of complexity for the trajectory behavior like Lyapunov exponents and topological entropy.

Our computational method allows us to thoroughly describe the bifurcations that the model (1) undergoes while transitioning between states: from tonic spiking to bursting and then to quiescence. Taken individually, each mapping offers only a glimpse into the system behavior. However, with an entire family of mappings we obtain deep insight into the evolution of the model's dynamics through the interplay and bifurcations of the fixed points and periodic orbits. This allows for not only the description of bifurcations *post factum*, but to predict the changes in the dynamics of the model under consideration before they actually occur. For additional analysis on elliptic bursters including torus formation, we refer the reader to [1].

References

1. Wojcik J. and Shilnikov A. Voltage interval mappings for dynamics transitions in elliptic bursters. *Physica D*, 240:1164–1180, 2011.
2. F. Argoul and J.C. Roux. Quasiperiodicity in chemistry: an experimental path in the neighbourhood of a codimension-two bifurcation. *Physics Letters*, 108A(8):426–430, 1985.
3. J. Rinzel. A formal classification of bursting mechanisms in excitable systems. In *Proc. International Congress of Mathematics ed A M Gleason (AMS) 157893*, 1987.
4. J. Rinzel and Y. S. Lee. Dissection of a model for neuronal parabolic bursting. *J Math Biol*, 25(6):653–675, 1987.
5. R. Bertram, M.J. Butte, T. Kiemel, and A. Sherman. Topological and phenomenological classification of bursting oscillations. *Bull.Math.Biol.*, 57(3):413–439, May 1995.
6. J. Guckenheimer. Towards a global theory of singularly perturbed systems. *Progress in Non-linear Differential Equations and Their Applications*, 19:214–225, 1996.
7. V.I. Arnold, V.S. Afraimovich, Yu.S. Ilyashenko, and L.P. Shilnikov. *Bifurcation Theory*, volume V of *Dynamical Systems. Encyclopaedia of Mathematical Sciences*. Springer, 1994.
8. E.F. Mischenko, Yu.S. Kolesov, A.Yu. Kolesov, and N.Kh. Rozov. *Asymptotic methods in singularly perturbed systems. Monographs in Contemporary Mathematics*. Consultants Bureau, New York, 1994.
9. A.N. Tikhonov. On the dependence of solutions of differential equations from a small parameter. *Mat. Sbornik*, 22(64):193–204, 1948.
10. A. I. Neishtadt. On delayed stability loss under dynamical bifurcations i. *Differential Equations*, 23:1385–1390, 1988.
11. L.P. Shilnikov, A.L. Shilnikov, D. Turaev, and L.O. Chua. *Methods of qualitative theory in nonlinear dynamics*, volume 1 and 2. World Scientific, Singapore, 1998, 2001.
12. F.N. Albahadily, J. Ringland, and M. Schell. Mixed-mode oscillations in an electrochemical system. i. a farey sequence which does not occur on a torus. *J. Chemical Physics*, 90(2):813–822, 1989.
13. P. Gaspard and XJ Wang. Homoclinic orbits and mixed-mode oscillations in far-from-equilibrium. *J. of Statistical Physics*, 48(1/2):151–199, 1987.
14. J.L. Hudson and D Marinko. An experimental study of multiple peak periodic and nonperiodic oscillations in the belousov-zhabotinskii reaction. *J. Chem. Phys.*, 71(4):1600–1606, 1979.
15. R.E. Griffiths and M.C. Pernarowski. Return map characterizations for a model of bursting with two slow variables. *SIAM J.Appl.Math.*, 66(6):1917–1948, 2006.
16. G.M. Medvedev. Transition to bursting via deterministic chaos. *Phys.Rev.Lett.*, 97:048102, 2006.
17. A.L. Shilnikov and M.L. Kolomiets. Methods of the qualitative theory for the hindmarsh-rose model: a case study. a tutorial. *International Journal of Bifurcation and Chaos*, 18(7):1–32, 2008.

18. P. Channell, G. Cymbalyuk, and A. Shilnikov. Origin of bursting through homoclinic spike adding in a neuron model. *Phys.Rev.Lett.*, 98(13):134101, March 2007.
19. P. Channell, G. Cymbalyuk, and A.L. Shilnikov. Applications of the poincare mapping technique to analysis of neuronal dynamics. *Neurocomputing*, 70:10–12, 2007.
20. P. Channell, I. Fuwape, A.B. Neiman, and Shilnikov A.L. Variability of bursting patterns in a neuron model in the presence of noise. *J Comput Neurosci*, 27(3):527–542, Dec 2009.
21. J. Doi and S. Kumagai. Generation of very slow neuronal rhythms and chaos near the hopf bifurcation in single neuron models. *J Comput Neurosci*, 19(3):325–356, Dec 2005.
22. M. Koper and P. Gaspard. Mixed-mode oscillations and incomplete homoclinic scenarios to a saddle-focus in the indium/thiocyanate electrochemical oscillators. *J. Chem. Physics*, 97(11):8250–8260, 1992.
23. M. Koper, P. Gaspard, and J. Sluyters. Mixed-mode oscillations and incomplete homoclinic scenarios to a saddle-focus in the indium/thiocyanate electrochemical oscillator. *J. Chem. Physics*, 97(11):8250–8260, 1992.
24. J. Su, J. Rubin, and D. Terman. Effects of noise on elliptic bursters. *Nonlinearity*, 17:133157, 2004.
25. A.L. Shilnikov. On bifurcations of the lorenz attractor in the shimizu-morioka model. *Physica D*, 62(1-4):338–346, 1993.
26. M.A. Kramer, R.D. Traub, and N.J. Kopell. New dynamics in cerebellar purkinje cells: torus canards. *Phys Rev Lett*, 101(6):068103, Aug 2008.
27. A.L. Shilnikov and N.F. Rulkov. Origin of chaos in a two-dimensional map modelling spiking-bursting neural activity. *International Journal of Bifurcation and Chaos*, 13(11):3325–3340, 2003.
28. C. Mira. *Chaotic dynamics from the one-dimensional endomorphism to the two-dimensional diffeomorphism*. World Scientific, Singapore, 1987.
29. N.K. Gavrilov and L.P. Shilnikov. On three-dimensional dynamical systems close to systems with a structurally unstable homoclinic curve. *Math.USSR Sb.*, 17(3):467–485, 1972.
30. M. A. Zaks, X. Sailer, L. Schimansky-Geier, and A. B. Neiman. Noise induced complexity: from subthreshold oscillations to spiking in coupled excitable systems. *Chaos*, 15(2):26117, Jun 2005.
31. M. Zaks. On chaotic subthreshold oscillations in a simple neuronal model. *Math. Model. Nat. Phenom.*, 6(1):1–14, 2011.
32. A.B. Katok. Lyapunov exponents, entropy and periodic orbits for diffeomorphisms. *Publ. Math. IHES*, 51:137–173, 1980.
33. P. Glendinning and T. Hall. Zeros of the kneading invariant and topological entropy for lorenz maps. *Nonlinearity*, 9:999–1014, 1996.
34. M.-C. Li and M. Malkin. Smooth symmetric and lorenz models for unimodal maps. *Int. J. Bifurcations and Chaos*, 13(11):3353–3371, 2003.
35. J. Guckenheimer. Singular hopf bifurcation in systems with two slow variables. *SIAM J. Appl. Dyn. Systems*, 7(4):1355–1377, 2008.
36. G. Cymbalyuk and A.L. Shilnikov. Coexistence of tonic spiking oscillations in a leech neuron model. *J Comput Neurosci*, 18(3):255–263, Jun 2005.
37. A. Kuznetsov, S. Kuznetsov, and NV. Stankevich. A simple autonomous quasiperiodic self-oscillator. *Commun Nonlinear Sci Numer Simulat*, 15:1676–1681, 2010.
38. A. Shilnikov and L. Shilnikov. Torus conditions in slow-fast models. *in preparation*, 2010.
39. N. Benes, A. Barry, T. Kaper, M. Kramer, and J. Burke. An elementary model of torus canards. *J. Chaos*, page submitted, 2010.
40. A. Neiman and A. Shilnikov. Spontaneous voltage oscillations enhance sensitivity of saccular hair cells. *J Neurophysiology (to be submitted)*, 2011.